MINISTERUL EDUCAȚIEI
UNIVERSITATEA TEHNICĂ
DIN CLUJ-NAPOCA

Mechanical Engineering

DOCTORAL THESIS
– SUMMARY –

Analysis of the mechanical behavior of 3D printed materials with applications in the automotive industry

PhD Student:
Eng. László RÁCZ

PhD Supervisior:
Prof. Eng. Mircea Cristian DUDESCU, PhD

Examination committee:
Chair: Prof. Eng. **Dan MÂNDRU**, Phd – Technical University of Cluj-Napoca;
PhD Supervisior:
Prof. Eng. **Mircea Cristian DUDESCU**, PhD - Technical University of Cluj-Napoca;
Members:
- Prof. Eng. **Liviu MARȘAVINA**, PhD – University Politehnica Timișoara;
- Prof. Eng. **Dan Mihai CONSTANTINESCU**, PhD - National University for Science and Technology Politehnica București;
- Prof. Eng. **Mihail HĂRDĂU**, PhD – Technical University of Cluj-Napoca.

– Cluj-Napoca –
2023

Table of contents

1. Introduction to 3D printing

1.1. Presentation of 3D printing technology

Three-dimensional printing is a process of constructing a solid three-dimensional object of any shape through an additive technological process by adding successive layers of material. Innovative 3D printing technology allows parts to be quickly created directly from a digital geometric model (CAD) without the need for additional equipment or assembly. Fused Deposition Modeling (FDM) is the manufacturing method used by affordable commercial 3D printers. By depositing discrete layers of extruded thermoplastic filament, FDM creates a 3D shape. The manufacturing technique can be used to quickly make both prototypes and functional components.

1.2. Examples of additive manufacturing

1.2.1. FDM – Fused Deposition Modeling

The FDM method is a 3D printing process invented by Scott Crump in 1989. It uses a layer-by-layer approach to create a conceptual design, which is saved in CAD format as an IGS or STL file. A slicer software is used to split the CAD files into horizontal layers, and the result is output as a G-code. The FDM process is guided by set parameters and is oriented towards the use of thermoplastic materials (polymers that turn into liquid, when heat applied). The filament is liquefied with heat in the extruder, and the liquid plastic is introduced onto the build platform via the extruder head. The process is repeated until the construction is complete.

1.2.2. SLA – Stereolithography

The SLA process, first invented in 1970 by Japanese researcher Hideo Kodama, is a modern stereolithographic fabrication method that uses ultraviolet light to solidify photosensitive photopolymers. Charles W. Hull, who invented the modern form of the machines, subsequently patented the technology in 1986 and co-founded 3D Systems. The process involves using a UV laser to polymerize the photopolymerized layers, with construction taking place in a resin pool. The process is repeated until the build or model is complete and may require specialised support materials.

1.2.4. PJP – PolyJet Printing

PolyJet Printing with Photopolymers (Material Jetting), patented by Objet Ltd. in 1999, combines inkjet technology with the use of photopolymers. It offers many advantages, including excellent resolution, smooth surfaces, a wide range of materials and colours, low cost and relatively short printing time. PolyJet is the name of any 3D printing technology that injects a liquid (build material) into a print head, which is then solidified by UV light. The PolyJet printing process is repeated until the object is complete. The raw material is stored in cartridges and connected directly to the nozzles. There can be multiple jet applicators, allowing different building materials to be sprayed simultaneously. This allows the creation of objects with different levels of flexibility within a single construction. PolyJet 3D printers can mix flexible and rigid materials to create designs with varying strength and flexibility.

1.3. The application scope of 3D printed parts as functional components

Three dimentional printing, also known as additive manufacturing, was originally developed as a rapid prototyping technique, but has evolved into a true manufacturing process. It offers many advantages over conventional manufacturing techniques, such as rapid

product customisation, greater design freedom, reduced waste and the potential to produce objects at reasonable prices. Understanding the design concepts and potential of the method is crucial for the best 3D printing decisions.

1.3.1. Components made by 3D printing in the automotive industry

Three dimentional printing technology has significantly changed the way industries design, develop and manufacture new products. In the automotive industry, these technologies have led to the development of complex and lightweight structures at the lowest possible cost. Although 3D printing is still mainly used for rapid prototyping in the development of new car models or concept cars, it has also been integrated into the production of some final components. The technology offers many advantages, such as producing small, accurate and fast prototypes, making prototypes in a very short time and transferring designs quickly to reality. Among the most common applications of 3D printing in the automotive industry are Formula 1 and Motorsport, printed vehicles, 3D prototypes, 3D spare parts and vehicle design studies. Recent developments include the introduction of a 3D printed components for a supercar by Lamborghini and Stratasys, which has reduced development time, production costs and vehicle weight.

2. Current status of the evaluation of the mechanical behavior of 3D printed materials

2.1. Process parameters influencing the properties of 3D printed materials

To determine whether 3D printed materials can be used for functional components, the mechanical properties must be determined and it is important to predict not only strength but also stiffness and how these relate to the parameters of the printing process. The main production parameters affecting the mechanical behaviour of FDM manufactured components that have been identified and investigated can be summarised as follows:

- Print direction (build orientation): refers to the orientation of the part on the platform.
- Bead width: is the width of the filament deposited by the FDM nozzle.- Layer thickness: The thickness of the deposited bead.
- Filament raster angle/filament orientation (raster angle): is the direction of the filaments relative to the X-axis of the build table.
- Raster width: The width of the raster pattern used for the inside of the parts.
- Air gap: The space between two adjacent filaments on the same layer.
- Number of contours: The filament deposited along the edge of the part.

2.2. Mechanical testing of 3D printed materials

2.2.1. Analysis of mechanically loaded FDM parts

Several publications and studies can be found in the literature presenting different methods and techniques for modelling 3D printed prototypes by FDM. In the FDM manufacturing process, it is observed that the mechanical strength of the components (such as tensile strength, flexural strength) and surface roughness are highly anisotropic. The strength, roughness and geometric accuracy of the final manufactured parts depend on various process parameters such as contour width, raster angle, raster width, layer thickness, part orientation, air gap and machine settings. The influence of deposited material temperature, raster width, air gap, raster angle and material colour on the tensile strength of the samples was also investigated. The influence of these parameters was investigated using both experimental techniques and numerical and analytical modelling techniques. Analysis of the temperature inside the printer (build chamber), the extrusion temperature and the width

of the extruded filament on the bonding quality of adjacent filaments in the FDM process are important factors influencing the increase of the contact area between filaments and their bonding.

2.2.2. Analytical model based on composite theory

Several publications and studies can be found in the literature presenting different methods and techniques for modelling 3D FDM printed structures. Particularly important for our study is the method presented by L. Li and Q. Sun, who proposed a method for representing 3D FDM printed structures as composite materials. ABS parts made by FDM processes essentially consist of partially bonded ABS filaments. The mechanical properties of FDM parts are governed by their mesostructures (the structure at the scale of the extruded filaments), which are determined by manufacturing parameters including filament width, layer thickness, deposition orientation and the dimensions of the spaces between the filaments. By selecting the manufacturing parameters, FDM processes can produce elements with the desired properties. To fully exploit this potential, aspects of the manufacturing process and mechanical properties of FDM parts should be investigated. Among the manufacturing parameters, the deposition directions of the layers and the dimensions of the spaces between the filaments are the most important parameters for controlling the mechanical properties. Thus, it is essential to establish material models of FDM parts in relation to these two manufacturing parameters. The models can then be used to design parts with the desired mechanical properties via locally controlled properties.

2.2.3. Simplified analytical model of the mechanical behaviour of FDM models

Another analytical model important for our study was presented by Croccolo, et al. The analytical model was developed according to several assumptions, namely: according to ASTM D638-10 standard FDM specimens can be considered as thin beams whose length is much greater than the width and height, consequently, it seems reasonable to assume an infinite length of the specimen gauge; as the external load is applied, the calibrated area of the specimen deforms with a uniformly distributed deformation.The calibrated area consists of a series of simplified elements formed by bars whose characteristics are defined appropriately for each type of specimen. In each of these elements, the total load is divided between the longitudinal and inclined layers so that their axial elongation is kept constant. In other words, all the bars cooperate to support the total load, working in parallel.

2.2.4. Finite element analysis of FDM materials

In the paper presented by Garg, A. and Bhattacharya, A. , finite element modeling and simulation for an acrylonitrile butadiene styrene (ABS) FDM specimen is performed using the ABAQUS finite element (FE) package. The specimens are designed at three different layer thicknesses (0.178, 0.254 and 0.330 mm) and three filament orientation angles (0°, 90° and 0°/90°) using CAD Pro/Engineer 5.0 modeling software. The models created are exported to ABAQUS in STEP file format. Overall dimensions for tensile test specimens are determined according to ASTM D638. The geometric model of the FDM specimen is prepared by generating layers at different tilt angles for different material thicknesses. Instead of using the theoretical circular cross-section of the layers, after deposition, the layers are placed in an elliptical cross-section with intra-layer overlapping or necking effect. The "necking" effect is a time-dependent diffusion phenomenon that takes its final form after solidification of the model. In addition, a region of overlap is observed between two adjacent filament layers, known as interlayer necking. These measurements are used to generate a more realistic geometric model of the FDM specimen. To build the whole model, the cross-section is created using microscopic measurements and then patterns (in terms of thickness and filament gap) are generated to prepare a rectangular model. The method presented by de Garg, A. and

Bhattacharya, A., leads to some conclusions about the relationship between the manufacturing process settings (filament height and raster orientation) and the mechanical properties of the resulting material.

3. Influence of printing parameters on the static behaviour of 3D printed materials

3.1. Main process parameters influencing the mechanical behaviour of 3D printed materials

This chapter aims to analyse the tensile properties of specimens created with a regular FDM 3D printer and to evaluate the technical parameters (printing software and pre-processing settings) on the mechanical properties of the printed specimens. The main parameters to be considered are the different printing orientations and patterns, percentage and infill rate. The main process parameters influencing the production of 3D FDM parts are infill rate, size and filament size, number of contours, build orientation and infill pattern. "The "infill pattern" can be variable and can change according to the infill percentage (1-100%). The pattern will not change with increasing infill percentage but only the "density". The printing software defines the infill patterns, different software offers different patterns.

3.2. Experimental analysis of the effect of raster orientation, infill rate and infill pattern on the mechanical properties of 3D printed materials

The study investigates the impact of process parameters on the mechanical characteristics of 3D printed FDM parts. A geometric model is created using CAD modelling tools and transferred to a stereolithographic file (STL) to start the FDM printing process. The resulting geometry is then converted to G-code using Simplify3D processing software. The Wanhao Duplicator i3 printer was used for FDM printing. The material used was ABS filament, a material commonly used for FDM parts. The mechanical properties of ABS filament are Ef=2140 MPa, σf=43 MPa, and specific tensile strain εf=2.7%. The geometrical model of the 3D printed specimens is made according to ISO 527-2-2012. Uniaxial tensile tests were performed to investigate the mechanical properties of the 3D printed material. The specimens were tested in an INSTRON 3366 universal testing machine with a capacity of 10 kN. A uniaxial extensometer was used to measure the specific strain. Three types of specimens were created using different parametric variations: a) infill rate, b) infill pattern and c) filament orientation.

To determine the mechanical properties of 3D printed specimens and the variability of these properties when different printing parameters are used, this study investigated the relationship between infill rate, infill pattern and filament (raster) orientation with tensile strength, specific strain corresponding to tensile strength and Young's modulus. A set of five specimens of each of the above mentioned variable combinations was printed and subjected to tensile testing. Figure 3.1 shows the variation of specific tensile strain at maximum stress (tensile strain), tensile strength and Young's modulus (tensile modulus) as a function of fill rate for the apparent cross-section.

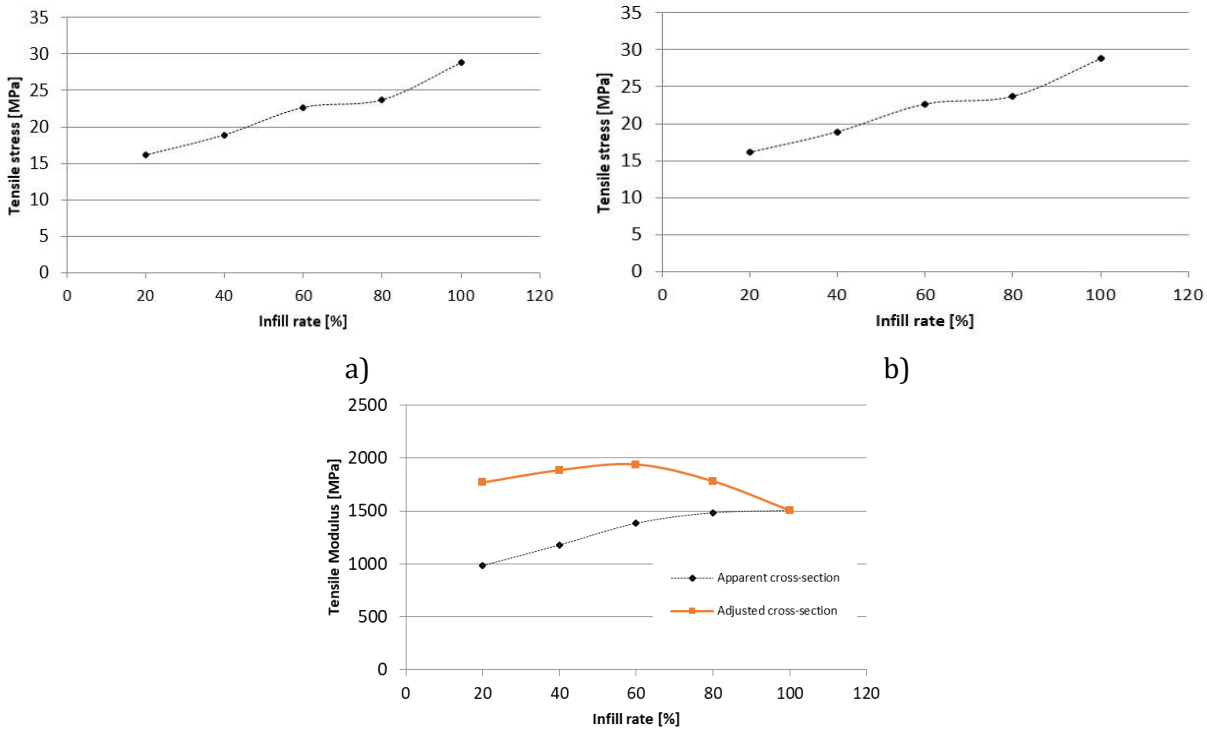

Figure 3.1 Variation with infill rate: a) tensile strength, b) tensile strain for maximum stress and c) modulus of elasticity (Young's modulus)

The influence of the infill pattern was studied on specimens printed with 100% infill rate and the following patterns: straight 0° and 90°, grid 0°-90° and 45°-45°, fast honeycomb, full honeycomb, triangular (60°) and wiggle. Figure 3.2 shows the variation of specific tensile strain, tensile stress and Young's modulus (tensile modulus) as a function of the infill pattern, given the apparent cross-section area.

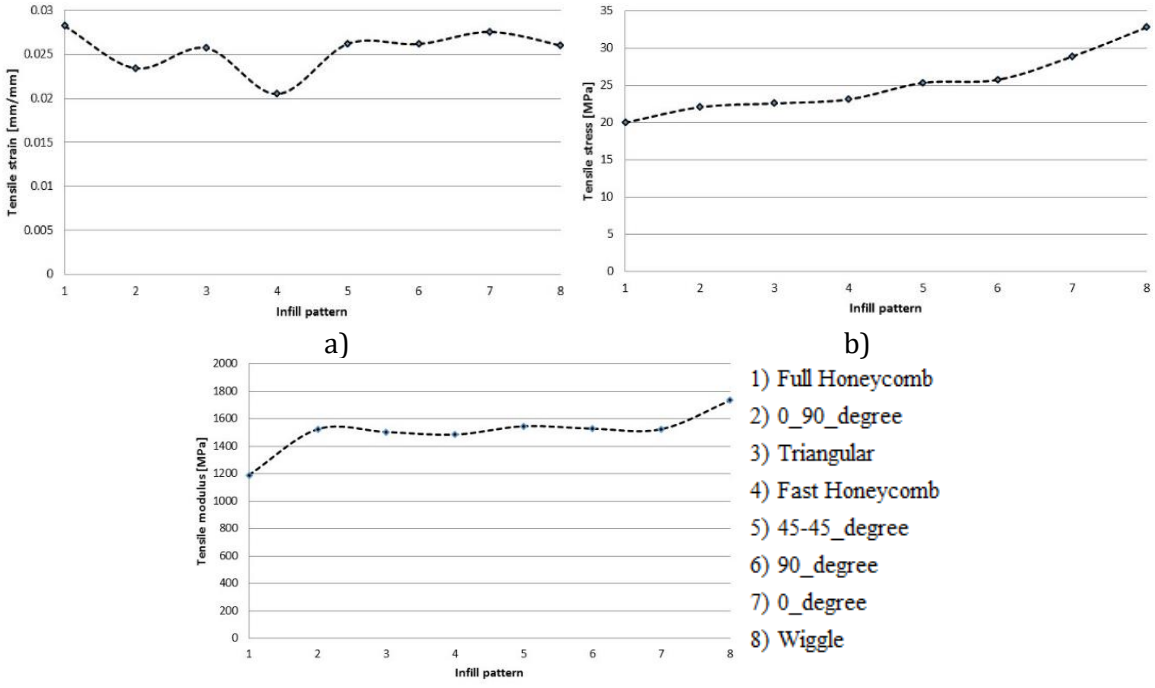

Figure 3.2 Variation as a function of infill pattern for: a) tensile strength, b) tensile strain at maximum stress c) Young's modulus

Specimens with a 100% fill rate and straight pattern orientation were printed by placing them at various angles around the X-axis of the printing platform, including 0°, 30°, 45° and 90°. Figure 3.3 shows the variation of tensile strength, specific tensile strain at maximum stress and Young's modulus as a function of raster orientation, given the apparent cross-section area.

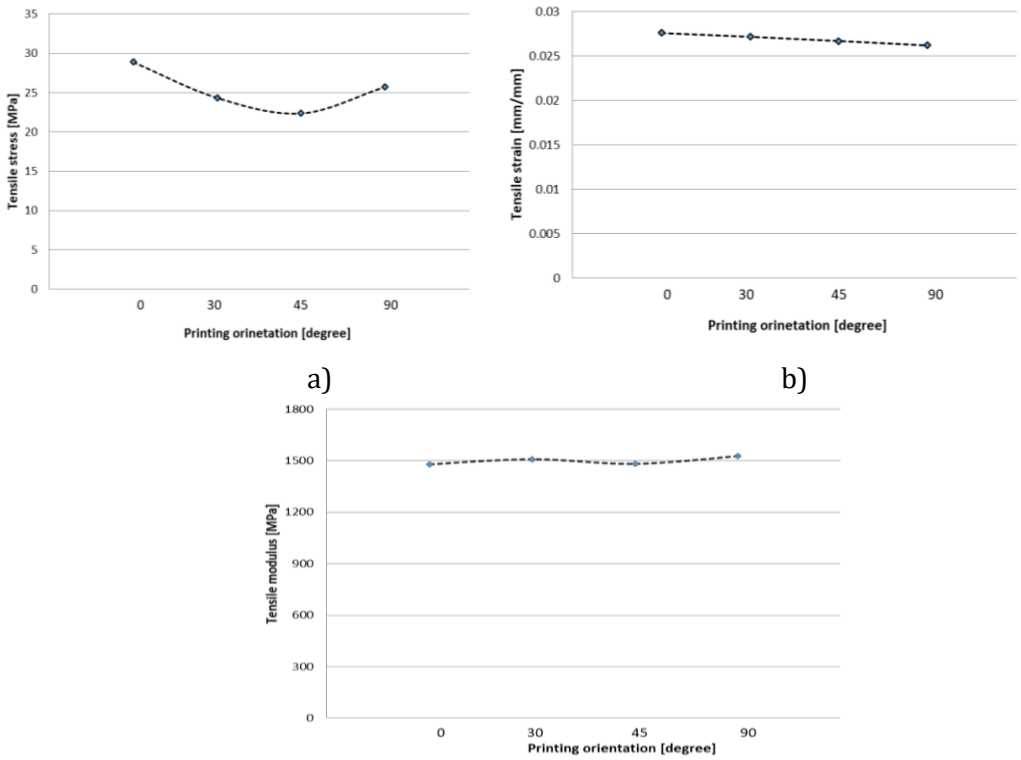

Figure 3.3 Variation as a function of raster orientation for a) tensile strength, b) tensile strain at maximum stress and c) modulus of elasticity

The mechanical properties of ABS specimens printed using FDM technology are significantly influenced by the infill rate, infill pattern and orientation of the specimens. Even though some specimens have been printed with a 100% infill rate, the actual air to material rate should be determined or estimated more accurately. The effect of specimen geometry on local stresses and strains will affect the mechanical behaviour of the material. The apparent modulus of elasticity increases with the percentage print rate, while the adjusted E-modulus takes into account the density of the specimens and should have a more constant behaviour around the ABS filament's value. The differences can be explained by approximate calculations of the actual cross-sectional area, which does not take into account the number of contours around the edges of the specimen. The orientation of the raster along the print direction leads to the highest tensile strength.

3.3. Applied analytical model of a specimen with simplified grid structure

The analytical model presented previously in paragraph 2.2.3 was studied on a model of a tensile specimen with 100% fill rate and a +45°-45° grid infill model made of ABS and used in the study described in paragraph 3.2. The implementation of the analytical model was carried out in Microsoft Excel, in the following the input parameters of the model and the resulting values are described. The input data were obtained by analysing the printed specimens as well as the information from the printer software. Comparing the results of the maximum normal stress with those measured experimentally for specimens having 100% fill rate and the +45°-45° grid filling model having an average value of σexp=25.36 MPa, a good convergence of these results with a relative deviation value of 4.36% was found, which

validates the analytical model developed by Crocolo. The model is based on the introduction of correction forces, which are experimentally determined to ensure the accuracy of the model. Factors such as material change, process parameters such as printing speed, printing temperature influence the adhesive forces between filaments and the implied results of the analytical model.

3.4. Influence of fill rate on mechanical properties of 3D printed materials - numerical investigation

This subchapter presents a novel method for simulating 3D printed parts manufactured by FDM printing. The method relies on the original G-code of the 3D printer to generate unique filaments. Based on the experimental evaluation of the cross-sectional geometry of a printed tensile specimen, the connection between filaments (inter- and intra-layer necking) is determined and the effect of filament flattening can also be determined. Uniaxial tensile tests were performed to investigate the mechanical property of the 3D printed material. Stress calculations were performed based on the outer dimensions of the tensile specimen without considering the material/air void ratio in the cross-sectional area. The resulting E-modulus will not correspond to reality, but the specific strain could serve as a reference for the validation of the proposed geometrical models and the corresponding numerical simulations. The methodology was applied for specimens with different infill ratios (20%, 40%, 60%, 80% and 100%) and the variation of elastic modulus E and tensile strength were determined.

3.4.1. Analysis of the geometric mezzo-structure of FDM printed specimens

After careful study of the method developed by Garg et al., a drawback to its real-life applicability was identified, namely that the method does not take into account the shell of the printed part. In real-life applications, it is not possible to print parts without the shell area if the fill rate is very low, e.g. 20%. Given the lack of a specific test standard for 3D printed materials, this was done by choosing specimens similar to plastics, given their widespread use and acceptance for 3D printed specimens. Figure 3.4 shows a cross-section of a 3D printed ISO_527 1A tensile specimen, in which both infill and shell areas can be distinguished. To identify the actual material area in the cross-section of a printed specimen, a new and improved model is required. In this study, the effectiveness of a geometric method has been analysed and a methodology has been devised to construct a highly realistic geometric model of printed parts, in which the ratio of material to voids is clearly identifiable in a virtual model. This geometric model should be suitable to undergo a fast meshing process, where the printed mesostructure will be transformed into finite elements, thus facilitating the prediction of the mechanical behaviour of printed parts using FEM analysis.

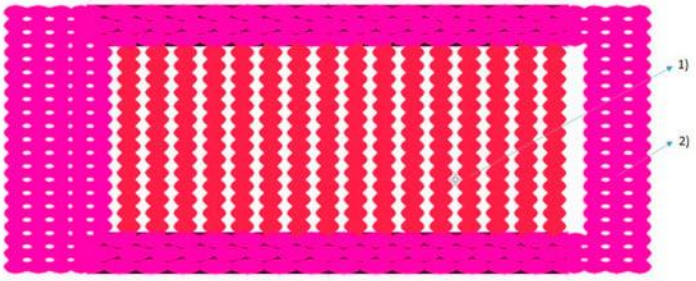

Figure 3.4 Infill section (1) and shell section (2) of a 3D printed tensile specimen type ISO_5271A

The virtual tensile specimen was constructed in ANSA according to the procedure described above. Initially five tensile specimen models were studied according to ISO_527 1A, in which the infill rate varied from 20% to 100%, the printing direction was kept the same, 0

degrees along the longitudinal axes of the specimens. Cross-sectional area extraction for tensile specimens was performed in ANSA. In order to verify the surface area determination method using a CAD model in ANSA, a microscopic study of the printed specimens is required.

3.4.2. Estimation of contact areas of printed filaments

To determine the actual shape and structure of the fibres the cross-section, mesostructure and infill pattern of the printed specimens were analysed under a microscope with a magnification factor of 50×. The result of the cross-section extraction from the geometric model was compared with the microscopic images of the printed specimens. Since the extruded filament is in a semi-fluid state, both the top and bottom of the filament flatten slightly when deposited on the front layer, as shown in the microscopic photograph in Figure 3.5a. The correlation of the geometrical area is necessary because the cross-section of the filaments is represented as a perfect ellipsoid in the geometrical model; however, in reality, the cross-section of the fibers has a larger contact area due to the fact that their cross-section is not perfectly ellipsoidal in shape, as shown in Figure 3.5b.

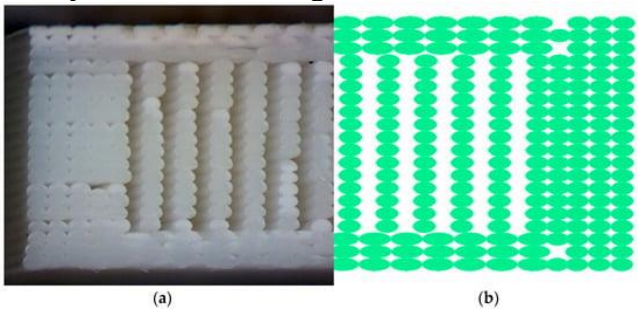

Figure 3.5 Comparison of the fibre structure of the cross-section between a 3D printed tensile specimen and the geometric model in ANSA: (a) printed specimen (microscope view); (b) geometric model

The flattening effect leads to the formation of larger contact areas between the filaments, known as intra- and inter-layer necking. This can be determined using optical measurements or by adjusting the thickness of the printed material and the number of layers. In the geometric model, the fibre cross-section is considered to be perfectly ellipsoidal and can be stabilised by determining the relationship between the printing parameters and the set dimensions. The model has been updated to maintain the perfect ellipsoidal representation of the filaments, but the contact area has been adjusted to allow measurement of intra-layer and inter-layer necking. This update allowed a more accurate determination of the fiber cross-sectional area. In order to validate the method, the test results under real conditions, in particular the specific tensile strain, will be compared with the numerical simulation result, validating the geometrical model.

3.4.3. Finite element analysis of 3D printed specimens

The finite element analysis was performed on the geometric models described in section 3.4.1. In order to validate the proposed geometric model, the result of the finite element analysis and the experimental data must match. In order to verify the cross-section of the specimens, a numerical simulation will be performed on the geometrical models, where the specific tensile strain will be compared with the experimentally obtained values.

The process used in this study starts with the initial geometric model, constructed with a conventional design tool. The CAD model will be processed in a "slicing tool" software, where the printing parameters are defined. The result of this process will be a G-code, which can be read by 3D printers. The G-code contains all the information the 3D printer needs, such as the temperature of the extrusion head, the height and width of the layer, the printing speed and, most importantly, all the coordinates of the movements of the extrusion heads. These coordinates and printer settings can

be used to create a very realistic microstructure model, using a plug in script in Ansa, which is suitable for finite element analysis. After determining the cross-sectional area of the tensile specimen, a finite element analysis was performed on a portion of the parallel side of the tensile specimen. To reduce simulation time, only one segment of the tensile specimen was analyzed. Several simulations were performed to determine the optimal modelling procedure. Factors influencing the result are element type, element order, element length and element quality. The first five sets of models (with infill rates of 20%, 40%, 60%, 80%, 100%, 0° direction along the longitudinal axis of the sample) were constructed using Tetraeder elements, first order, with a generic element length of 0.05 mm. To analyze the effect of element length on simulation accuracy and time, a different model configuration was tested. The element length was doubled from 0.05 (FEA1) to 0.1 (FEA2) mm. After examining the effects of FE model construction parameters, simulation and post-processing tools, it can be concluded that the best practice for our FE analysis investigation is the following: the Tetraeder element model of order 1 with an overall element length of 0.1 mm.

3.4.4. Validation of simulation results by tensile tests

The geometric models of the 3D printed specimens were made in accordance with ISO 527-2-2012. Uniaxial tensile tests were performed to investigate the mechanical properties of the 3D printed material. A uniaxial extensometer was used to measure the tensile stress. For each infill rate, a number of five specimens were tested. The material used for the preparation of the specimens was acrylonitrile butadiene-styrene ABS filament. The tensile strength calculation is based on the cross-sectional dimensions of a specimen (4 mm thickness, 10 mm wide). The tensile strain can serve as a reference for the validation of the geometrical model using numerical simulations. The simulation was performed using Epilysis software and the same specimens were tested experimentally. The results can be summarized in Table 3.1, where the experimentally measured tensile strain is compared with the results of FEM simulations performed with smaller element length FEA1 (0.05 mm) and larger FEA2 (0.01 mm) and the deviation between them is expressed in percentages. The results are selected from the elastic range of the material (specimen) at a load of 160 N.

Table 3.1 Comparison of displacements from experimental tensile test (EXP) with simulation results with two different element lengths (FEA1 and FEA2)

Infill rate [%]	Tens.Strain EXP [mm/mm]	Tens. Strain FEA1 [mm/mm]	Tens. Strain. FEA2 [mm/mm]	Relative deviation FEA1 -EXP [%]	Relative deviation FEA2 -EXP [%]	Relative deviation FEA1 -FEA2 [%]
20%	0.004040	0.003917	0.003796	3.14	6.43	3.09
40%	0.003520	0.003300	0.003250	6.65	8.31	1.53
60%	0.003040	0.002907	0.002866	4.57	6.06	1.40
80%	0.002740	0.002584	0.002561	6.04	6.97	0.87
100%	0.002510	0.002323	0.002310	8.06	8.66	0.56

Ten simulations were performed to determine the effect of element size on the accuracy of the result. The results showed a difference of minimum 3.13% and maximum 8.05% for the FE model with discretization having element length of 0.05 mm (FEA1) compared to the experimental result (EXP). The results obtained are consistent with the measured data, which demonstrated that our estimates of the contact areas and filament shape of the printed specimens and the proposed finite element models are accurate and can be successfully used further on. In the case of FEA1 and FEA2, the cross-sectional area was extracted from the geometric model in ANSA, as shown in Table 3.2, and entered into the test machine software, allowing a more accurate calculation of normal stresses and hence tensile strength. The increase in cross-sectional area of FEA1 and FEA2 is, on average, 13%, so that a 20% increase in fill rate does not lead to a similar increase in cross-section. One possible

explanation is that a change in the fill rate not only causes an increase in the amount of filament deposited, but is also constrained by the arrangement (pattern) of filaments in relation to the part geometry.

Table 3.2 Estimated cross sections according to infill rate and mesh lenght

Infill rate	Area of the cross-section [mm^2]	
	FEA1	FEA2
20%	20.50	20.30
40%	23.85	23.35
60%	27.05	26.52
80%	30.23	29.66
100%	34.72	34.19

To determine the tensile modulus of elasticity of the 3D printed specimen with different infill rates, the cross-section extracted from the geometric model was fed back into the test machine software and the results were recalculated according to the two sets of values. In Table 3.3, the tensile modulus (E) result is shown, where: modulus E-EXP represents the tensile modulus of the specimen - determined experimentally - considering the full cross-section of the specimen; modulus E-FEA1 and FEA2 represent the recalculated tensile modulus of the specimens using the extracted area from the geometric model using finer discretization (0.05 mm) and coarser discretization (0.1 mm), respectively.

Table 3.3 Modulus of elasticity of printed specimens with geometrically determined cross-section

Infill rate	Modulus of elasticity E (MPa)		
	FEA1	FEA2	EXP
20 %	1916.00	1934.90	982.00
40 %	1974.80	2017.10	1,177.50
60 %	2046.70	2087.70	1,384.10
80 %	1983.40	2021.50	1,498.90
100 %	1703.40	1729.80	1,521.80

The influences of the perimeter length on the cross-sectional area (which translates into E modulus values) are shown in Figure 3.6. It can be seen that there is an inverse correlation between the numerically determined and experimentally determined E modulus in relation to the infill rate. For a low infill rate of 20%, the difference between the E EXP modulus and the FEA1 E modulus is 53%, while for a 100% infill rate, the difference between the E EXP modulus and the FEA1 is reduced to a still significant value of 36%. It can be concluded that, for the tensile modulus of elasticity, using the entire cross-section of the 3D printed specimen, even for a 100% infill rate, will not give a result within a predictable error range. The results clearly show that a 20% increase in infill rate does not directly translate into a 20% change in elastic modulus. For the experimental results, the difference from EXP Infill_20% to EXP Infill_40% represents a step of 19.9%, but this is reduced to 2.1% when comparing EXP Infill_80% to EXP Infill_100%. Notably, FEA1 and FEA2 values are increasing up to Infill_60%, then slightly decreasing up to Infill_100%.

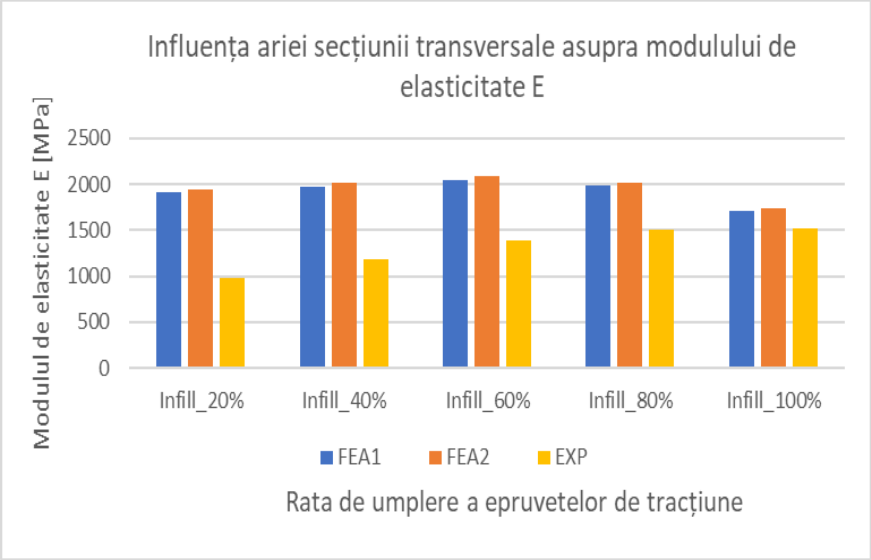

Figure 3.6 Modulus of elasticity values for different infill rates recalculated from numerically estimated cross-sectional areas

In this chapter 3D printed tensile specimens were analysed to understand the effect of different infill rates on mechanical behaviour. The results obtained allow the following general conclusions to be drawn:

- The proposed approach to build a complex finite element model based on the G-code generated by the printer's software is a reliable methodology to predict the behavior of FDM printed parts, but adjustments are needed to represent intra- and inter-layer necking to obtain accurate results.
- The cross-sectional area of a tensile specimen extracted from the numerical model is predicted with good accuracy and allows estimation of specific stress-strain curves and elastic moduli closer to reality.
- For higher filling rates, the tensile strength and modulus of elasticity values of the specimens converge towards the experimentally obtained values, but not proportionally.
- The results clearly show that increasing the filling rate does not directly translate into a corresponding change in the modulus of elasticity, as the arrangement of the filament rows influences the bonding forces between them and the outer shell.

3.5. Influence of infill pattern on mechanical properties of 3D printed materials

In order to study the effect of the infill pattern, numerical models were constructed using the same script that generates a geometric model from G-code (as described in the previous chapter). The mesostructure of the printed specimen cross-section was analysed under a microscope to determine the actual shape and structural interaction of the filaments. The cross-sectional structure of the filaments in the numerical model was compared with detailed images of the printed specimens. Finite element analysis (Epilysis solver) was used to simulate a tensile test and was performed on different specimens corresponding to the 6 infill patterns analyzed, namely: 0°-90° and ±45° grid, 60° triangular, fast honeycomb, full honeycomb and wiggle. All patterns correspond to a 100% infill rate, so theoretically have full cross-section. The same boundary conditions were applied to the numerical model as to the real specimens during the tensile test. To validate the method, tensile tests under real conditions are required, where the experimentally determined specific tensile strain will be compared with the result of the numerical simulation. The results are summarised in Table 3.4, where the experimentally measured tensile strain is compared with the FE simulation results, the results being selected from the elastic range of the stress-strain curve.

Table 3.4 Values of the tensile strains obtained by numerical simulations vs. determined experimentally

Infill pattern	Tens. Strain EXP (mm/mm)	Tens.Strain FEA (mm/mm)	Relative deviation. FEA-EXP (%)
Grid 0-90	0.00259	0.00277	6.95
Grid +45-45	0.00267	0.00269	0.75
Fast Honeycomb	0.00279	0.00285	2.15
Full Honeycomb	0.00333	0.00351	5.40
Tria 60°	0.00274	0.00294	7.2
Wiggle	0.00223	0.00205	8

The cross-sectional area extracted from the geometric model was re-entered into the test machine software and the stress results were recalculated according to the new value. Based on the fitted stress-strain curves, the elastic modulus value E for each infill model was recalculated, and their comparative values with the original ones based on the full cross-section are shown in Table 3.5.

Table 3.5. E modulus values for different infill patterns

Infill pattern	Modul of elasticity E (MPa)		Relative deviation (%)
	Calculated (numerical)	Full Cross-section	
Grid 0-90	2049.00	1523.7	25,4
Grid +45-45	1631.00	1545.2	5,3
Fast Honeycomb	1892.04	1484.0	21,6
Full Honeycomb	1272.20	1188.6	6,6
Tria 60°	2055.26	1502.8	26,8
Wiggle	1877.49	1733.5	7,7

Figure 3.7 shows the comparative results in the form of a bar graph of the tensile modulus of elasticity for different infill patterns. The modulus of elasticity value E (denoted E_Fcs) is the measured modulus of elasticity of the specimen using the full cross-sectional area (Fcs), and the other value is the modulus (denoted E_Calc) based on the corrected cross-sectional area. It can be concluded that the use of the full cross-section of 3D printed specimens, even for a 100% fill rate, will not give for the E modulus and ultimate tensile strength a result within a reasonable error range, especially for designs such as grid 0-90°, fast honeycomb and triangular 60°.

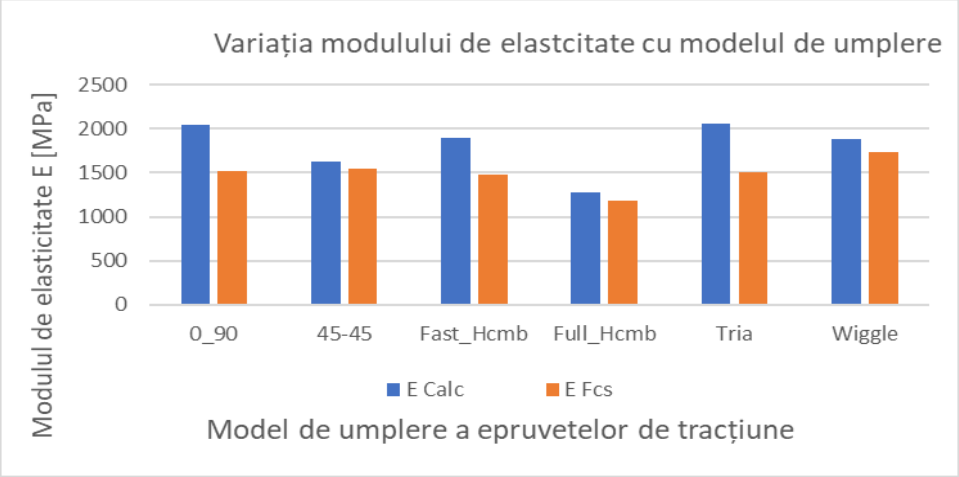

Figure 3.7 Comparative results of modulus of elasticity with and without cross-sectional area adjustment for different infill designs

The results presented in paragraph 3.5 allow the following general conclusions to be drawn:

- The proposed methodology of constructing a finite element model from the G-code generated by the printer is a reliable method of evaluating the influence of the interior structure given by the infill pattern on the mechanical behaviour of FDM printed parts.
- To obtain accurate results, adjustments to represent intra- and inter-layer necking are required and must be performed on real printed specimens.
- The cross-sectional area of a tensile specimen extracted from the numerical model is predicted with good accuracy and allows the estimation of specific stress-strain curves and E-modules closer to reality.
- Models such as ±45° grid, full honeycomb and wiggle have a higher ratio of material to air voids and gave reasonable results in terms of tensile strength and E-modulus compared to specimens considered full cross-section, so it would be recommended to be used for printed parts subjected to mechanical stresses.
- Designs such as 0-90° grid, fast honeycomb and 60° triangular show 20% higher differences in tensile strength and E-modulus when the cross-section is considered full, which cannot be neglected for printed parts under mechanical stress.

4. Influence of printing parameters on the dynamical behaviour of 3D printed materials

4.1. Evaluation of impact properties of 3D printed materials

To determine whether 3D printed materials can be used for functional components, the mechanical properties must be determined and it is also important to predict not only strength, stiffness, but also impact resistance and how these are related to process parameters. Studies show that specimens produced by FDM have significantly lower impact strength than those produced by injection moulding technology. Material discontinuities, which are an effect of the deposition of the material in layers and the method of filling the layers, have a significant influence on the overall strength of the product. Where possible, the FDM process should be designed to minimise discontinuities and cavities within the product, which are most vulnerable to failure.Another problem is damage to 3D printed components due to impact on structural integrity. The data obtained show that the impact resistance exhibited by 3D printed composites is significantly higher than that of regular 3D printed thermoplastics, and in some cases even better than that of regular prepregs.

Fifit five specimens were manufactured using ABS filament (Plasty Mladeč, Czech Republic). The geometry of the specimens was constructed in SolidWorks 2016 using standard dimensions according to EN ISO 179-1: 2000, (for thermoplastics), type C, using a V-shaped notch at an angle of 45° ± 1°. Specimen dimensions are: l=80mm, b=10mm, a=4mm.

Each set consisted of five specimens for a given process parameter. Since the mechanical properties of several thermoplastic materials can vary with ambient temperatures, the tests were performed according to room temperature standards. Shock bending (Charpy) tests were performed to study the energy absorption of different specimen configurations.

4.1.1. Influence of the infill rate

The influence of fill rate on the resilience of the specimens was studied on specimens printed with a straight 0^o direction (relative to the longitudinal axis of the printer). After testing each specimen, the following properties were measured and recorded: resilience, break energy value, angle variation, impact velocity and related statistical values. The most important factors for our analysis are the mean of the values, the standard deviation and the nature of the breakage, whether the specimen is completely or only partially broken. The results are presented in Table 4.1. where the mean resilience values (kJ/m2) of the printed specimens are shown for different fill rates. As expected, the direct correlation between

resilience and fill rate was confirmed. The result showed that the resilience of 3D printed parts, (and the ability to absorb more energy) increases with increasing infill percentage of the tested specimens.

Table 4.1 Average resilience values for specimens printed with the same infill pattern and different infill rates

Sample	CH-0-20%	CH-0-40%	CH-0-60%	CH-0-80%	CH-0-100%
Resiliece [kJ/m²]	74,185	9,71	13,015	15,347	16,708

4.1.2. Influence of the infill pattern

The influence of the infill pattern was studied on the second set of samples. The specimens were printed using the same material and printer settings, except that the infill pattern was changed. Six different infill patterns were used: 0^o-90^o grid, -45^o+45^o grid, fast honeycomb, full honeycomb, wiggle and 60^o triangular. The results of the impact tests were the average resilience values of the samples printed with the same infill rate but with a different infill pattern, shown in Table 4.2.

Table 4.2 Average resilience values for specimens printed with the same 100% infill rate but different infill patterns

Infill pattern	Grid 0-90	Grid 45±45	Tria	Fast HC	Full HC	WIG
Resilience [kJ/m²]	5,687	6,919	6,936	8,22	9.76	12,36

To get a better overview of the impact performance of the test specimens, the impact test results are arranged in ascending order in Table 4.3.

Table 4.3. Mean values of sample resilience in ascending order

Nr.	**Sample**	**Average resilience [kJ/m²]**
1	CH_0-100%	16,71
2	CH_0-80%	15,35
3	CH_0-60%	13,02
4	CH_WIGGLE_100%	12,36
5	CH_FULLHC_100%	9,76
6	CH_0-40%	9,71
7	CH_FASTHC_100%	8,22
8	CH_0-20%	7,42
9	CH_TRIA_100%	6.94
10	CH_45+45-100%	6,92
11	CH_0-90-100%	5,69

In this chapter the influence of the infill rate and infill pattern on the resilience of 3D printed specimens was investigated. Two sets of specimens were analysed. The first set consisted of specimens printed with the same filling pattern but with a infill rate ranging from 20% to 100%. The second set of specimens were manufactured with the same infill rate, all at 100%, but the infill pattern was different for each of them. The mechanical behaviour of

dynamically tested 3D printed materials was investigated by impact (Charpy) tests on standard specimens to determine the resilience of the material. A noticeable improvement in resilience is observed when the infill rate is increased from 40% to 60% (3.3 kJ/m2), much higher than when the range is increased from 20% to 40% (2.3kJ/m2). Overall, the best resilience characteristics in our test had the sample printed with a 100% infill rate and wiggle infill pattern. With the same 100% infill rate, the 0°-90° grid pattern printed sample has 2.9 times less impact resistance. It is found that the resilience changes relatively little from sample to sample in the same category. The impact tests indicate that, in addition to the fill rate, the result is significantly influenced by the infill pattern. The best result can be estimated, based on our experience with infill models having the filament structure in the transverse direction versus dynamic load.

4.2. Effect of the infill pattern on fatigue characteristics of 3D printed materials

insight in fatigue behavior and its deterioration mechanisms are essential for evaluating polymeric materials fabricated by FDM in various applications to determine their long-term durability and reliability. In addition to process parameters, mechanical factors characteristic of fatigue testing, such as stress amplitude, strain, average stress, cycle asymmetry coefficient, specific stress-strain ratio, stress cycle frequency, self-heating, stress concentrators, etc., are of interest.

In this sub-chapter, the effect of infill pattern on fatigue stress of standard 3D printed ABS specimens was investigated. Standard specimens with eight types of infill patterns were subjected to static and cyclic tests. After completion of tensile tests to obtain the ultimate tensile stress (UTS), axial fatigue tests were performed with pulsating cycling with a skewness coefficient R = 0.1 and a sinusoidal waveform to evaluate the influence of the infill patterns on the number of cycles to failure for five different stress levels. Based on the S-N curves a mathematical model of the fatigue curves is presented. Comparative results of the S-N curves for different infill patterns, number of cycles for a given stress ratio (%UTS) and examination of the failure zone allow conclusions and main results of the study to be formulated. Since there are no material standards for AM manufactured materials, standard specimens were printed according to ASTM D638 with 100% infill rate and the following patterns: rectilinear 0° and 90°, grid 0°-90° and +45°-45°, fast honeycomb, full honeycomb, triangular (60°) and wiggle type. The initial tensile test and fatigue tests were performed on a servo-hydraulic testing machine type Instron 8810 at room temperature.

4.2.1. Fatigue test

Axial fatigue tests in accordance with ASTM D7791 were performed on ten specimens for each infill pattern. A frequency study (15 Hz, 10 Hz, and 5 Hz) was performed on the 0° infill pattern to determine the best frequency to perform the fatigue tests. On the one hand, a higher frequency reduces the testing time, but on the other hand, the specimen will start to heat up. The average temperature of the specimen over the calibrated length was monitored with a thermal camera only for the high loading level, corresponding to a stress level of 90% of the tensile strength (UTS). A test frequency of 10 Hz was chosen to perform cyclic loading. A pulsating fatigue cycle with a sinusoidal waveform and a cycle asymmetry coefficient R=0.1 was selected for the experimental procedure.

Fatigue lifetimes for maximum stress values of 90% UTS, 75% UTS, 60% UTS, 45% UTS and 40% UTS were measured for each type of specimen with different infill patterns, with a number of two specimens being tested for each level. The aim was not to determine fatigue level, but rather to observe the influence of the internal structure of the specimens on fatigue life span. The results of S-N curves plotted considering the maximum cycle stress as a percentage of the tensile strength are shown in Figure 4.1 for different models of curve-fitted infill.

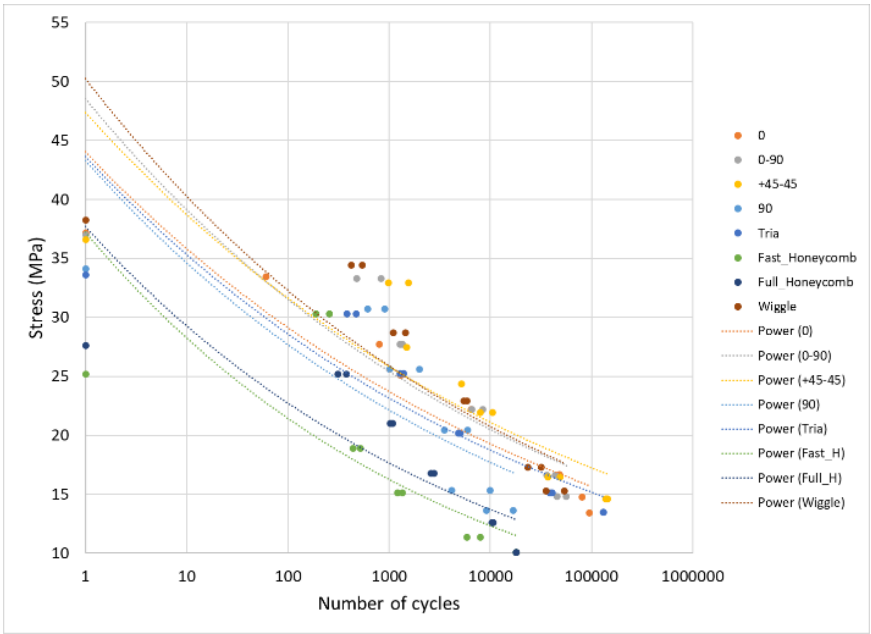

a)

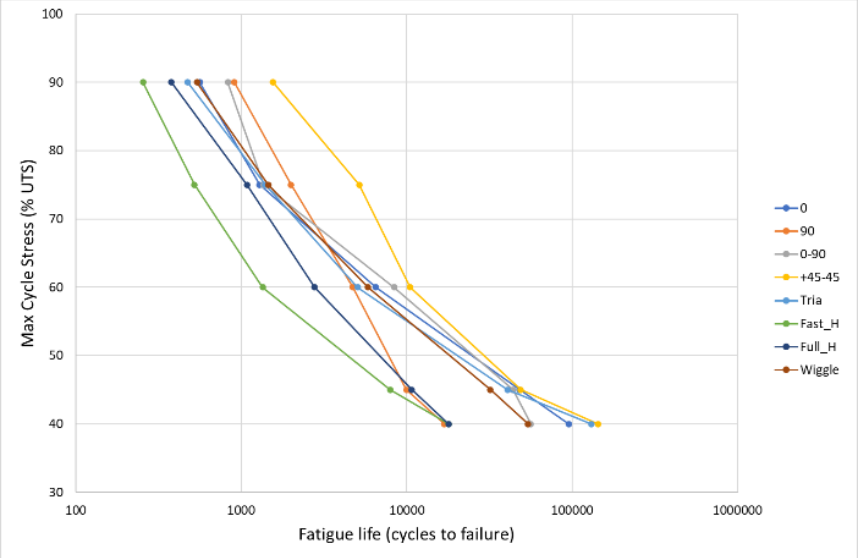

b)

Figure 4.1 (a) S-N curves for different infill patterns; (b) S-N curves with normalized stress.

A simple mathematical model for the determination of fatigue properties was developed on the basis of stress-number of cycles (S-N) curves:

$$S = 10^{A} * N^{B} \quad (4.1)$$

where A and B are coefficients determined by the method of least squares and presented in Table 4.6.

Table 4.6 Linear model coefficients and approximation accuracy

Infill pattern	Rectilinear 0°	Rectilinear 90°	Grid 0°-90°	Grid ±45°	Tria 60°	Wiggle	Fast Honeycomb	Full Honeycomb
A	1.627	1.636	1.686	1.675	1.639	1.701	1.571	1.576
B	-0.08	-0.09	-0.09	-0.08	-0.09	-0.09	-0.11	-0.10
	219	706	356	781	172	598	99	98

R-square	0.904	0.572	0.759	0.747	0.829	0.767	0.642	0.697
RMSE (MPa)	0.1290	0.2360	0.1771	0.1791	0.1488	0.1738	0.2628	0.2141

It is found that for a given stress value the lifetime (number of cycles at a stress of 15 MPa) of the different infill patterns is different (Table 4.7)

Table 4.7 Service life span of different infill models

Infill Pattern	Rectilinear 0°	Rectilinear 90°	Grid 0°-90°	Grid ±45°	Tria 60°	Wiggle	Fast Honeycomb	Full Honeycomb
NR. of cycles	80739	4154	56161	143204	1344	5120	40550	35500

The results indicate that designs with filaments inclined with respect to the direction of load (grid ±45°, straight 0° and triangular 60°) have a longer fatigue life span compared to those with most filaments perpendicular to the direction of the load (fast honeycomb, full honeycomb and straight 90°). Designs such as 0°-90° grid and wiggle are very close to the first group, having filaments inclined or along and perpendicular to the tensile direction (0°-90° grid). Fractographic analysis using electron microscopy (SEM) revealed the microstructural phenomena that produced specimen breakage and provided additional information about microstructural interaction between filaments and filament breakage in cyclic loading. By examining SEM images of specimens with filament orientation other than 0° (loading direction), it can be concluded that the fatigue behavior depends more on other parameters, such as intra- and interlayer bond strength and void density, than on the strength of the ABS monofilament. For some designs, such as fast honeycomb and full honeycomb, the air gap is significant, the interlaminar bonds are low, which explains the poorer fatigue results.

The results presented in this chapter allow the following general conclusions to be drawn:

- Designs with filaments inclined around the tensile axis (grid ±45°, rectilinear 0° and triangular (60°)) have high fatigue life compared to those with most filaments perpendicular to the tensile direction. (fast honeycomb, full honeycomb and straight 90°).
- 3D printed materials with different infill patterns exhibit different static and dynamic properties, materials with higher tensile strength may have a lower number of cycles to fatigue failure.
- The position of the filaments within a layer and the arrangement of the layer in relation to adjacent layers and the direction of loading are defining for fatigue life.
- Intra- and interlayer bonding and material density (material/air void ratio) play a key role in the dynamic behaviour of FDM materials.

5. Case studies

5.1. Mechanical behavior of 3D printed variable stiffness beams

The mechanical properties of parts manufactured by Fused Deposition Modeling are significantly influenced by the printing parameters. Creating models with a variable infill rate and infill pattern would have a number of advantages over conventionally 3D printed models. Firstly, a better weight-to-strength ratio could be achieved by optimising the internal structure to suit the requirements of use. In less stressed areas, the fill rate can be reduced and in high stress areas, the fill rate can be increased to better withstand loads. In this way, a

significant amount of material and printing time can be saved. The mechanical behaviour of 3D printed parts is also influenced by the infill pattern in combination with the infill rate.

5.1.1. Manufacturing process of specimens with variable infill rate

In order to create parts with a variable infill rate or variable infill pattern, we had to find a method that allowed us to set a different print configuration within a single part. The solution tested was to divide a geometric volume into its sub-volumes. Sub-volumes are needed to clearly define the boundaries within a part, where the different print configuration can be applied. For our study, we set out to analyze the effect of fill rate on 3D printed parts printed with 0o direction (along the longitudinal axis of the sample) and variable fill rate. The fill rate variation will be symmetrical to the center of the specimen, i.e. 20%-40%-60%-80%-100%-80%-60%-40%-20%. The results of the measurements will then be compared with the result of another set of specimens printed with a uniform fill rate of 100% with a print direction of 0^o - along the longitudinal axis of the specimen.

5.1.2. Experimental study

Three sets of specimens were printed (by FDM method using ABS material) and tested. One set was printed with regular uniform settings, using a 100% infill ratio and a grid pattern, with 0^o direction in line with the longitudinal axes of the bending specimens. The second set of specimens was printed with a variable fill ratio, (20%-40%-60%-80%-100%-80%-60%-40%-20%), as previously described, where the thin partition wall was maintained between the different fill ratio scenarios. The third set of specimens was printed according to the same fill percentage distribution, but without the thin walls separating the different infill scenarios. Each set of tested specimens contained five 3D printed samples. The specimens were tested for 3-point bending under a static load. The test results are summarised in Table 5.1.

Table 5.1 Results of three-point bend tests of printed specimens

Specimen type	Modulus (MPa)	Flexture stress at max. load (MPa)	Flexture load (N)	Deflection at max. load (mm)
Uniform 0-degree, 100%	1,984.00	53.67	95.42	7.414
Variabil_Version1	2,078.20	45.26	80.46	3.942
Variabil_Version2	2,004.40	48.76	86.69	4.917

5.1.3. Finite element analysis

Finite element analysis was performed on printed specimens to determine the accuracy of predicting the mechanical behavior of 3D printed parts using standard FEM methods. It is very difficult to predict the mechanical behaviour of 3D printed parts without testing them using experimental methods. A two-model approach was used to determine the most appropriate method for analysing 3D printed samples. The first modelling approach used a 2nd order Tetraida solid element discretisation with element sizes ranging from 0.5-1.5 mm. The model was loaded with a force of 60 N, applied in the middle of the bending specimen. The quality of the elements was checked against NASTRAN standard requirements. The model was subjected to a standard linear-static simulation using the Epylisis solver. Figure 5.1 shows the result of the FEM simulation of the Tetraida model, where a) represents the beam arrow as a function of load direction (maximum2,770 mm), b) the distribution of normal stresses.

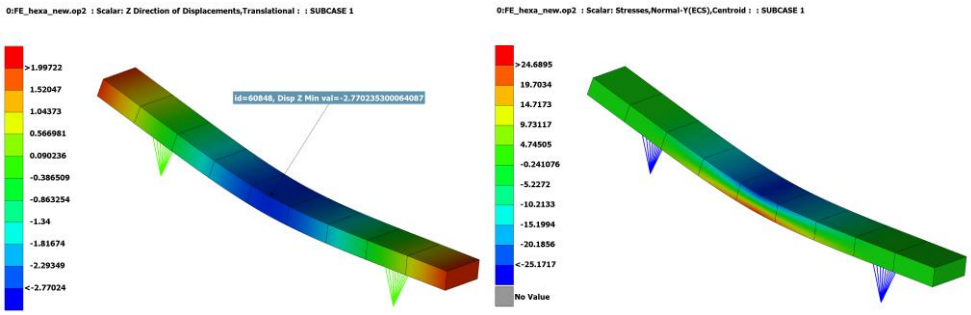

Figure 5.1 FEM analysis results of the Hexaeder model; a) beam arrow, b) normal stress distribution

It can be seen that the results are almost identical, with only ~0.4% difference between them. The execution time for the more complex second-order Tetraeder model was 10.8 seconds, while the Hexaieder model compiled in 1.5 seconds.

5.1.4. Analytical calculation of the deflection of a beam with variable mechanical properties

The calculation of the analytical beam deformation was done by energy methods, i.e. using Castigliano's second theorem. The loading scheme is shown in Figure 5.2 and consists of a simply resisted beam loaded with a concentrated force placed halfway across the beam span. The different regions of the beam that have different elastic moduli E2-E5 are marked by their openings. Identical dimensions to those for the experimental analysis are chosen: a=5 mm, half-length l=30 mm, F=60 N. The moduli of elasticity correspond to different filling rates, E1 = 1901 MPa - 20% filling rate; E2 = 1974 MPa - 40% filling rate; E3 = 2052 MPa - 60% filling rate; E4 = 1983 MPa - 80% filling rate; E5 = 1703 MPa - 100% filling rate. Cross section dimensions are 10 mm width and 4 mm thickness.

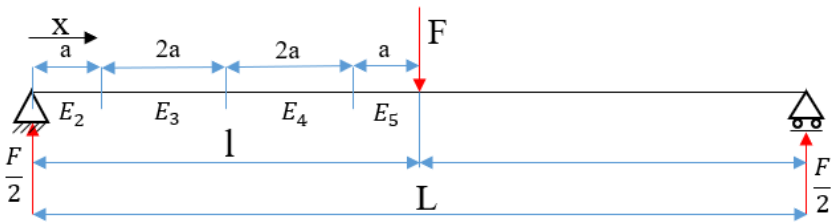

Figure 5.2 Schematic representation of the analytical model

Substituting the dimensions and material constants above, we get an arrow value of 2.72 mm.

The study investigated the effect of varying print rates on the mechanical behaviour of 3D printed ABS parts. Simplify 3D software was used to determine the printing parameters. Three sets of five specimens were subjected to a three-point bending test. The revised model improved the bending strength by 7.5%, from 80.46N to 86N, and the maximum deflection increased by 25%. The specimen printed with a uniform print rate had the best performance in terms of strength and deflection. The material cost was about 13% and the difference in maximum deformation was 51%. The Tetraeder model was used to determine the best method to predict the mechanical behavior using FEM analysis. The results showed a difference of 4-10% between the experimental results and the FE analysis results. Improved FDM parts could be an economical and efficient method for creating well-optimized parts in terms of weight strength while minimizing material usage.

5.2. Analysis of a 3D printed brake pedal for a vehicle

5.2.1. Reverse engineering of the pedal model

Based on the methodology and results presented in the previous chapters, it has been demonstrated that it is possible to produce 3D printed parts with a functional role under certain conditions. The major advantage of the method is that one-off or small series parts can be produced in a short time and at low cost from a CAD model or using the advantages of reverse engineering.

To demonstrate these concepts, this chapter presents the study of a brake pedal from a Dacia Duster car, using additive technologies, i.e. FDM. A plastic pedal (ABS) made by injection moulding was purchased from the Dacia network. A reverse engineering process was carried out on the basis of this pedal, i.e. it was optically scanned using a scanning system based on the Atos Core fringe projection model produced by GOM in Germany. The scanning system is shown in Figure 5.3 and has a maximum accuracy of 2 microns.

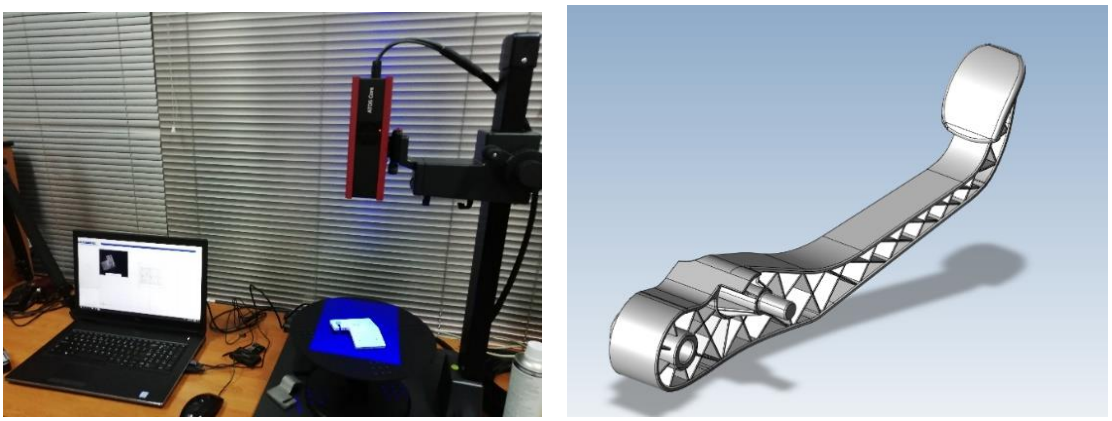

Figure 5.9 CAD model of the pedal: a) Atos Core 3D optical scanning system, b) CAD model resulting from the generation of the

Based on the CAD models, two models of the pedal with 100% filling degree and the filling pattern recommended by the printer for maximum strength, i.e. Grid +45°-45°, were produced by 3D printing on a STRATASYS Fortus 450mc industrial printer.

5.2.2. Analysis of the mechanical behaviour of 3D printed pedals by electrical resistive tensometry

In order to analyse the mechanical behaviour of the 3D printed pedals in relation to the injected model used on the Dacia Duster vehicle, a test stand has been created to allow for similar pedal resonance and pedal stress conditions to those existing in reality. HBM 1-LY1x-6/120 type tensile transducers with 6mm base and 120 Ohm resistance were bonded. HBM Spider 8 measuring bridge and CatMan Easy v.3.2 analysis and evaluation software were used to determine the specific strains. The transducers were mounted in half-deck, with one transducer being active and the other used for thermal compensation. Figure 5.13 shows the pedals analysed as well as the mounting and positioning of the resistive tensor transducers.

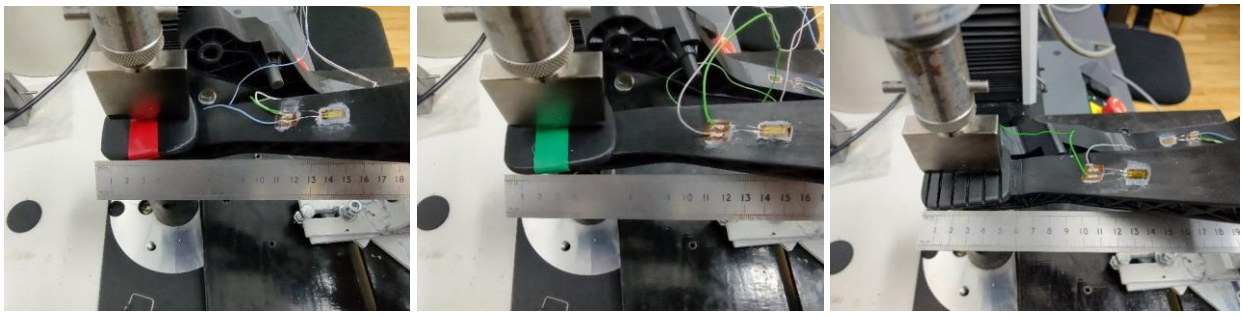

a) b) c)

Figure 5.13 Measurement of specific pedal deformations by resistive electrical tensometry: a) printed pedal with filaments oriented along the longitudinal axis, b) printed pedal with filaments oriented transversely, c) commercial injected pedal

Measurements for the same value of applied force, i.e. similar positions of the transducers in relation to the applied force position, resulted in the values summarised in Table 5.2.

Table 5.2. Specific strain values measured on different types of pedals.

Pedal type	**Applied load (N)**	**Tensile strain (µm/m)**
Longintudinal orientation	19.2	428
Transversal orinetation	19.2	453
Injection molded	19.2	99,8

In order to carry out a comparative study of the results obtained experimentally, pedals with similar mechanical characteristics (Table 5.3) were analysed numerically using the finite element method, i.e. a single set of mechanical characteristics was used for the 3D printed pedals, without taking into account their modification in relation to the orientation of the pedal (build orientation) in the workspace of the 3D printer.

Table 5.3 Mechanical characteristics used in numerical models

Material	**Modul of elasticity (MPa)**	**Poisson's ratio**	**Density (g/cm3)**
Injected pedal	7375	0.35	1.57
3D printed pedal	1452	0.39	1.05

It is observed that there is a small difference (5.5%) in the specific strain for 3D printed pedals, with the model where the filaments are oriented longitudinally being slightly stiffer compared to the one with transverse filaments. The commercial version of the plastic injection moulded pedal is much stiffer (more than 4 times), with a higher modulus of elasticity. The numerical results show good convergence with the experimental results, with relative deviations of 13% for the longitudinal filament printed pedal, 7.3% for the transverse filament printed pedal and 2.2% for the homogeneous material pedal.

The results obtained for this case study demonstrate on the one hand the need to carry out tests or simulations of 3D printed materials in order to determine as close as possible to reality their mechanical characteristics, and uniform distribution of the material inside the 3D printed elements and on the other hand demonstrate the possibility of replacing in the future some complex parts made today by conventional technologies with printed elements having mechanical characteristics that allow them to fulfil a functional role.

6. Final conclusions

6.1. General conclusions

This study investigated the mechanical properties of 3D printed ABS parts using a set of manufacturing parameters that play a crucial role in the mechanical properties of 3D printed parts. The study focused on the influence of printing parameters on the static and dynamic behavior of 3D printed materials. A new modeling method was developed to estimate the mechanical properties of 3D printed parts. The results of the experimental study and the results of the finite element method simulation were compared to validate the modelling method tested in this study.

The literature review revealed that there are several approaches to create a predictive model aimed at estimating the mechanical characteristics of 3D printed specimens. The most important methods for our study were found in the research presented by L. Li and Q. Sun, Croccolo, et al. and by Garg, A. and Bhattacharya, A.. L. Li and Q. Sun proposed a method for calculating elastic constants in a group of filaments printed as a laminate, in which the mechanical properties can be controlled by local properties. They used equations to determine the constitutive patterns of FDM parts, varying deposition densities, orientations and combinations to produce the required stiffness properties. The study provides insight into the relationships between filaments and air gap determination. However, it is limited in its applicability due to the lack of shell sections and is not capable of processing complex infill patterns. Croccolo et al.'s research focused on the effect of contour on the strength and static stiffness of FDM printed parts. They developed a closed-form predictive model, which was tested for ultimate strength and Young's modulus. The final model showed good agreement, confirmed by small errors in strength prediction, modulus of elasticity and verifiable stiffness.
In the chapter entitled: **Simplified applied analytical model of a specimen with grid-type filling** pattern, the method was analysed in detail and the following conclusions were reached: the method is not able to relate to a low filling rate, if individual filaments do not touch each other, because the whole model is based on the introduction of correction coefficients for the adhesion force, the experimental determination of which is necessary for the accuracy of the model. In the work taken by Garg, A. and Bhattacharya, A., FEM modeling and simulation is carried out and realistic models are developed considering layers of different thicknesses and filaments at different angles, keeping the bonded region between and among the layers.

The influence of printing parameters on the static behaviour of 3D printed materials presents in detail the main process parameters that influence the mechanical behaviour of 3D printed materials by the FDM method. The main process parameters influencing the result of FDM 3D printing (for the same material) are: infill rate, layer height and width, number of layers (contours), build orinetation and infill pattern.
Experimental analysis of the effect of raster orientation, fill rate and fill pattern on the mechanical properties of 3D printed materials investigates the impact of the above mentioned parameters on the physical characteristics of the FDM 3D printed part. To determine the mechanical properties of 3D printed specimens and the variability of these properties when different printing parameters are used, this study analyzed the relationship between infill rate, infill pattern and filament (raster) orientation with tensile strength, specific strain corresponding to tensile strength and modulus of elasticity.
The study continued with the **investigation of the influence of the fill rate on the mechanical properties of 3D printed materials** (numerical investigation). The mechanical behaviour of 3D printed tensile specimens was studied to better understand the effect of varying fill rates. A novel approach for the analysis of 3D printed FDM models has been presented, which uses a geometric model built on the printer output G-code to facilitate finite element analysis.

The findings presented in this paper allow the following general conclusions to be drawn:
- The proposed approach for building a complex finite element model based on the G-code generated by the printer pre-machining software is a reliable methodology to predict the behavior of FDM printed parts.
- The cross-sectional area of a tensile specimen extracted from the numerical model is predicted with good accuracy.
- For higher infill rates, the tensile strength and modulus of elasticity values of the specimens converge to the experimentally obtained values, but not proportionally.
- The results clearly show that increasing the infill rate does not directly translate into a corresponding change in the modulus of elasticity.

The influence of the filling pattern on the mechanical properties of 3D printed materials is also very important to study in order to understand the effect of internal structure on mechanical behaviour. An innovative method for creating numerical models of parts based on the G-code generated by the printer has been described, which helps in finite element analysis and evaluation of the problem of air gap (voids) to material ratio.
Based on the data reported in this paper, the following general conclusions can be drawn:
- The proposed methodology for building a finite element model from the G-code generated by the printer is a valid method for evaluating the influence of the interior structure provided by the infill pattern on the mechanical performance of the parts produced by FDM.
- In order to obtain accurate results, adjustments must be made to reproduce intra- and interlayer necking on real printed specimens.
- The cross-sectional area of a tensile specimen taken from the numerical model has a high accuracy, which allows more accurate calculation of stress-strain curves and E-modules.
To determine whether 3D printed materials can be used for functional components, **the influence of printing parameters on the dynamic behaviour of 3D printed materials** must be determined. The mechanical behaviour of dynamically stressed 3D printed materials was investigated by impact bending (Charpy) tests on standard specimens to determine the resilience of the material. The impact tests indicate that in addition to the fill rate, the result is also influenced by the fill pattern. The best result can be estimated, based on our experience with infill models having the structure of the filaments in the transverse direction in relation to the dynamic load.

The effect of the filler pattern on the fatigue characteristics of 3D printed materials was studied on 3D printed tensile specimens (with eight types of filler patterns) that were subjected to static and axial fatigue tests to evaluate the influence of the infill patterns on the number of cycles to failure for five different stress levels.
The results presented in this paper allow to draw the following general conclusions on the effect of the infill pattern on the fatigue characteristics of 3D printed materials:
- The ±45° grid, 0° rectilinear and triughiular (60°) models have high fatigue life compared to fast honeycomb, full honeycomb and 90° rectilinear.
- Designs such as grid 0°-90° and wiggle are very close to the first group, having inclined (wiggle) filaments.
- 3D printed materials with different infill patterns have different static and dynamic properties.
- The position of the filaments within a layer and the arrangement of the layer relative to adjacent layers and to the direction of loading are defining for the fatigue behavior.
- Intra- and interlayer bonding and material density (material/air gap ratio) play a key role in the dynamic behaviour of FDM materials.

Mechanical behaviour of 3D-printed variable stiffness beams - is an important topic to investigate to determine the effect of variable infill rate on the mechanical behaviour of 3D-printed ABS parts. Comparing the test results, we can conclude that the effect of variable infill rate has a significant effect on the mechanical behavior of specimens. The

revised modeling method improved the flexural strength capacities of the variably printed specimens by 7.5%, from 80.46N to 86N. The deflection also increased by 25% from 3.9 mm to 4.9 mm. The printed specimen with a uniform fill rate of 100% had the best performance in terms of both strength and deformation.

In order to test the possibility of using 3D printed parts as functional parts we chose to continue with the **analysis of a car brake pedal made by 3D printing**. In this chapter, an injection moulded clutch pedal was analysed and compared with two 3D printed versions. It is observed that there is a small difference (5.5%) in the specific strain for 3D printed pedals, with the model where the filaments are oriented longitudinally being slightly stiffer compared to the one with transverse filaments. The commercial version of the plastic injection moulded pedal is much stiffer (more than 4 times), with a higher modulus of elasticity. The numerical results show a good convergence with the experimental results, with relative deviations of 13% for the longitudinal filament printed pedal, 7.3% for the transverse filament printed pedal and 2.2% for the homogeneous injected pedal.

6.2. Originality and innovative contributions of the thesis

This PhD thesis investigated the mechanical behaviour of 3D printed materials with applications in the automotive industry. The aim of this thesis was to develop a non-destructive method for predicting the mechanical behaviour of 3D printed parts intended for use in applications where they have to withstand different stresses, using finite element simulation.

The current state of knowledge in the field has highlighted several personal contributions:

- The most important parameters of the 3D printing process were identified and ranked according to their influence;
- Different types of prediction methods were analysed and their drawbacks were identified;
- Experiments were carried out on a 3D printer to understand its operation and to determine the possibilities offered by hardware and software settings.

This research has led to the conclusion that, although the subject is being intensively researched, it still offers great potential that has not yet been fully exploited.

The study of the influence of fill rate on the mechanical properties of 3D printed materials, presents the following innovations:

- Creation of a script for the ANSA pre-processing tool capable of reading geometric coordinates from a G-code and transforming them into a virtual replica of individually printed filaments;
- A modelling method that uses the 3D printer's G-code to build virtual CAD models;
- The modelling method is capable of building both the shell section and the filler section of 3D printed parts;
- A unique approach for determining the actual cross-sectional area for 3D printed FDM parts using a virtual modeling method was presented;
- Determination of elastic moduli for different infill rates and infill patterns using finite element simulation and experimental testing;
- Creating an equivalent material card for finite element analysis for each studied combination of fill pattern and fill rate (Simplified Material Card);
- Optimisation of the finite element modelling method in terms of quality and resource requirements/run time.

The analysis of the mechanical behavior of variable stiffness beams obtained by 3D printing, brings the following original contributions:

- The method of preparing the CAD model of test specimens in the Simplify tool to print parts with multiple print settings;
- Model configuration to eliminate the separation barrier between different printer settings.

6.3. Prospects for further development

Research can be pursued along the following lines:
- Determining the influence of other process parameters of the printing process (part orientation. Extrusion temperature, enclosure temperature, filament deposition speed, etc.)
- Numerical modelling of complex parts based on G-code with the introduction of all factors related to inter and intra layer interaction.
- Application of the presented methodology on elements made of several materials
- Optimization of the internal structure of printed parts by local modification of printing parameters.

LIST OF PUBLICATIONS

The results of this PhD thesis have been published as articles in indexed journals or in the proceedings of international conferences.

Published and indexed papers:

P1. **Racz, L.** & Dudescu, M. C. (2020). Evaluation of Impact Proprieties of 3D Printed Materials. *ACTA TECHNICA NAPOCENSIS-Series: APPLIED MATHEMATICS, MECHANICS, and ENGINEERING*, *63*(4). ISSN 1221-5872, WOS:000606612500014 (IF 2022: 0.3, Q4)

P2. **Racz, L.**, & Dudescu, M. C. (2022). Numerical Investigation of the Infill Rate upon Mechanical Proprieties of 3D-Printed Materials. *Polymers*, *14*(10), 2022. eISSN: 2073-4360; DOI: 10.3390/polym14102022, WOS:000803270500001 (IF 2022: 5, **Q1**)

P3. Dudescu C., **Racz, L.**, Popa, F. (2022) Effect of Infill Pattern on Fatigue Characteristics of 3D Printed Polymers, Material Today: Proceedings 2022, ISSN 2214-7853, https://doi.org/10.1016/j.matpr.2022.11.283 (SCOPUS)

P4. Dudescu, C., & **Racz, L**. (2017). Effects of raster orientation, infill rate and infill pattern on the mechanical properties of 3D printed materials. *ACTA Univ. Cibiniensis*, *69*(1), 23-30. DOI: 10.1515/aucts-2017-0004 (SCIENDO)

P5. **Racz, L.**, & Dudescu, M. C. (2021). Mechanical behavior of beams with variable stiffness obtained by 3D printing. In *MATEC Web of Conferences* (Vol. 343, p. 08014). EDP Sciences. DOI: 10.1051/matecconf/202134308014 (ProQuest, DOAJ, Google Scholar)

Works in publication:

P6. **Racz, L.**, & Dudescu, M. C. (2023) Numerical evaluation of the infill pattern upon mechanical proprieties of 3D printed materials, International Conference Structural Integrity and Reliability of Advanced Materials obtained through Additive Manufacturing – SIRAMM23, Timisoara, Romania, 8th –11th March 2023 – se va publica in Procedia Structural Integrity (ELSEVIER/SCOPUS)